Journal of
Radiation Protection and Research 2023;48(4):167–174
https://doi.org/10.14407/jrpr.2023.00080

pISSN 2508-1888 | eISSN 2466-2461

Material Discrimination Using X-Ray and Neutron

Jaehyun Lee, Jinhyung Park, Jae Yeon Park, Moonsik Chae, Jungho Mun, Jong Hyun Jung

Advanced Radiation Technology Institute, Korea Atomic Energy Research Institute, Jeongeup, Korea

ABSTRACT

Background: A nondestructive test is commonly used to inspect the surface defects and internal structure of an object without any physical damage. X-rays generated from an electron accelerator or a tube are one of the methods used for nondestructive testing. The high penetration of X-rays through materials with low atomic numbers makes it difficult to discriminate between these materials using X-ray imaging. The interaction characteristics of neutrons with materials can supplement the limitations of X-ray imaging in material discrimination.

Materials and Methods: The radiation image acquisition process for air-cargo security inspection equipment using X-rays and neutrons was simulated using a GEometry ANd Tracking (Geant4) simulation toolkit. Radiation images of phantoms composed of 13 materials were obtained, and the *R*-value, representing the attenuation ratio of neutrons and gamma rays in a material, was calculated from these images.

Results and Discussion: The *R*-values were calculated from the simulated X-ray and neutron images for each phantom and compared with those obtained in the experiments. The *R*-values obtained from the experiments were higher than those obtained from the simulations. The difference can be due to the following two causes. The first reason is that there are various facilities or equipment in the experimental environment that scatter neutrons, unlike the simulation. The other is the difference in the neutron signal processing. In the simulation, the neutron signal is the sum of the number of neutrons entering the detector. However, in the experiment, the neutron signal was obtained by superimposing the intensities of the neutron signals. Neutron detectors also detect gamma rays, and the neutron signal cannot be clearly distinguished in the process of separating the two types of radiation. Despite these differences, the two results showed similar trends and the viability of using simulation-based radiation images, particularly in the field of security screening. With further research, the simulation-based radiation images can replace ones from experiments and be used in the related fields.

Conclusion: The Korea Atomic Energy Research Institute has developed air-cargo security inspection equipment using neutrons and X-rays. Using this equipment, radiation images and *R*-values for various materials were obtained. The equipment was reconstructed, and the *R*-values were obtained for 13 materials using the Geant4 simulation toolkit. The *R*-values calculated by experiment and simulation show similar trends. Therefore, we confirmed the feasibility of using the simulation-based radiation image.

Keywords: Neutron, X-Ray, Material Discrimination, Air-Cargo, Security Inspection, Monte Carlo Simulation

Original Research

Received February 27, 2023
Revision August 8, 2023
Accepted September 13, 2023

Corresponding author: Jaehyun Lee

Advanced Radiation Technology Institute, Korea Atomic Energy Research Institute, 29 Geumgu-gil, Jeongeup 56212, Korea
E-mail: jaehyunlee@kaeri.re.kr
https://orcid.org/0000-0002-4923-3361

Introduction

In recent decades, a considerable effort has been put into systems related to baggage or cargo inspection to correspond to the increasing demand for cargo and passengers yearly. In particular, since the September 11, 2001 attack, a significant amount of bud-

get and manpower has been invested in reinforcing the aviation security system to ensure the safety and security of passengers and crew from terrorism and the aviation security screening process has become more comprehensive and stringent [1].

Radiation-based security screening, such as inspection equipment using two-dimensional X-ray radiography [2], three-dimensional computed tomography [3], neutrons [4], and artificial intelligence (AI) [5], has the advantage of being able to inspect baggage or cargo without opening them. X-rays are commonly used in many fields, such as aerospace, automotive, medicine, and construction, to detect defects, including cracks, voids, and inclusions, that are invisible to the naked eye [6, 7]. Especially, X-rays are the general source used to inspect objects for security purposes in places where safety and security are required, such as airports. However, security screening methods based on X-rays have the limitation of generating gray-scale images that only contain the shape of the object. Thus, it is difficult to distinguish objects in images based on their appearance and contrast, especially for objects made with low atomic number materials. Subsequently, a security screening method capable of distinguishing between organic and inorganic materials using dual-energy X-ray systems has been studied and applied to aviation security systems in many countries [8, 9]. The system using dual-energy X-rays also has limitations in accurately discriminating dangerous materials, such as explosives, chemical agents, nuclear materials and devices, and drugs.

Recently, as various criminal methods have been intelligently developed, the difficulty in security screening has increased. For this reason, accurate identification of hazardous materials that pose a threat to safety is essential and required in the field of security screening. Neutrons can help to distinguish objects with low atomic numbers, which is a limitation of X-rays, and many related studies have been conducted since the September 11, 2001 attack [10–12]. X-rays and neutrons show different characteristics in their interactions with matter, and this difference enables the discrimination of matter [13]. Because X-rays are electromagnetic waves that interact with the atomic electrons of matter, the interaction depends on the atomic number of the matter and the energy of the X-rays. In general, the penetrating power of X-rays on to materials is inversely proportional to the atomic number of elements that compose them. By contrast, neutrons have a neutral charge and are subatomic particles that interact with the atomic nuclei of the matter. Compared to X-rays, neutrons easily penetrate materials, such as heavy metals, and are easily scattered or absorbed by elements, such as hydrogen. Therefore, by using both X-rays and neutrons for security screening, it is possible to accurately discriminate materials.

The Korea Atomic Energy Research Institute (KAERI) developed security inspection equipment for air-cargo containers using X-ray and neutron sources to detect objects including explosives, chemical agents, nuclear materials, and drugs. Because the equipment uses X-rays and neutrons, it is possible to obtain the shape of the object inside the air-cargo as well as information on the materials that constitute the object.

In this study, we report the results of material discrimination for 13 materials through Monte Carlo method-based simulation and compare the results with experimental results. The security inspection equipment was reconstructed in the simulation in order to obtain radiation images. We used the *R*-value, which is the ratio of the attenuation coefficient of neutrons and gamma rays, to discriminate materials and was calculated from the radiation images. We aim to support the use of simulation-based radiation images by comparing the *R*-values of the experiments and simulations.

Materials and Methods

1. Air-Cargo Security Inspection Equipment

The air-cargo security inspection equipment developed by KAERI is composed of X-ray and neutron radiation sources, detector systems, a moving system, and an integrated control system. The X-rays and neutrons generated from each radiation source were detected by different detectors. The air-cargo was scanned while being moved by the moving system. The integrated control system remotely controlled radiation sources, moving system, signal acquisition, and other devices.

1) X-ray image system

X-rays are produced by isotopes or by accelerating electrons in devices such as tubes and radiofrequency (RF) accelerators. To examine inside an air-cargo, X-ray energy in the order of MeV is required, and an RF linear accelerator (RF linac) is employed. Electrons are generated in a triode-type direct current electron gun and accelerated to an energy of 6 MeV using a side-coupled RF linac. Accelerated electrons collide with a tungsten target of 2 mm thick to generate bremsstrahlung X-rays [14]. It can have any energy ranging

https://doi.org/10.14407/jrpr.2023.00080

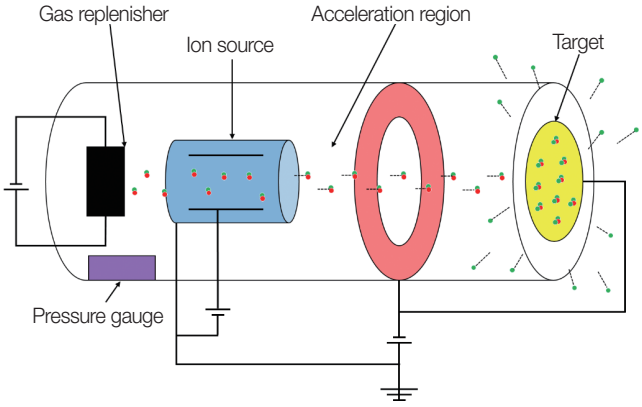

Fig. 1. Schematic of the deuterium-tritium generator consisting of replenisher, ion source, accelerating region, and target.

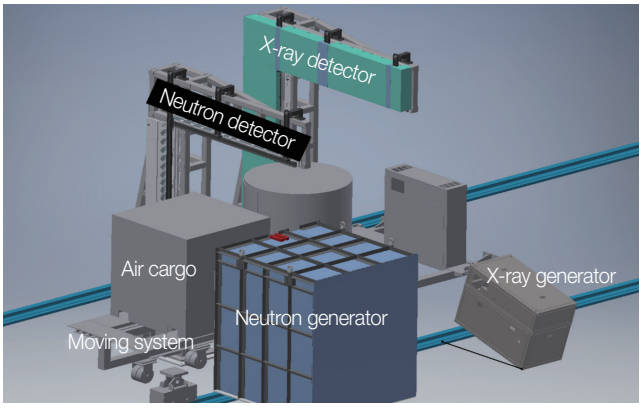

Fig. 2. Layout of the air-cargo security inspection system.

from zero to the maximum kinetic energy of electrons. A cylindrical collimator made of lead covers the target for shielding. There was a 10 mm-thick slit inside the collimator. Therefore, X-rays can be considered as a vertical fan beam separated by an angle of 23.4° and can enter the detector after passing through the air-cargo.

The detector module for X-rays consisted of $CdWO_4$ scintillators, Si-PIN photodiodes, and a control board (LCS 4.6; Detection Technology). It was composed of 2×32 channels vertically in one detector module, and a total of 30 detector modules were installed in the 'L' shaped frame. Therefore, there are 2×32 image pixels per X-ray detector module.

2) Neutron image system

A deuterium-tritium generator that emits anisotropic and mono-energetic neutrons with an energy of 14.1 MeV was used as a neutron source (Genie 35; Sodern). As shown in Fig. 1, the generator consists of a replenisher, an ion source, an accelerating region, and a target. Deuterium gas was inside the replenisher, and the gas was ionized by heating in the ion source. The ionized gas was extracted and accelerated by the high voltage in the acceleration region, and collided with the target containing tritium. This process resulted in a nuclear fusion reaction that produced alpha particles and neutrons, and fast neutrons with an energy of 14.1 MeV were emitted somewhat anisotropically from the target. To moderate and shield fast neutrons, a collimator of high-density polyethylene (HDPE) surrounded the neutron source. As with X-rays, the neutron collimator had a slit with 40 mm thick, through which neutrons are emitted.

The neutron detector module developed by the KAERI consists of plastic scintillators, a silicon photomultiplier (SiPM), and an analog-to-digital converter board. The module detects both neutrons and gamma rays, and the gamma rays must be removed as noise to obtain high-quality neutron images. A pulse shape discrimination (PSD) technique was applied to separate the neutron and gamma-ray signals [15]. A total of 23 detector modules composed of 2×8 channels vertically in one detector module were installed in the 'L' shaped frame (Fig. 2). Therefore, a neutron image of 2×184 pixels was acquired. The entire image was obtained while the air-cargo was moved by the moving system.

2. Simulations

GEometry ANd Tracking (Geant4; https://geant4.org/), a radiation transport simulation toolkit based on the Monte Carlo method, was used to describe experiments that acquired radiation images through the interaction between radiation and matter [16].

1) Geometry

Radiation images can be obtained by detecting the incident radiation on the detectors after the radiation emitted from the radiation sources interacts with the materials. To describe this process as a simulation, the radiation source, collimator, air-cargo, phantom for material discrimination, and radiation detector were reflected in the geometry.

X-rays can be produced when an electron beam accelerated by a linac up to 6 MeV energy collides with a 2 mm thick tungsten target. Therefore, a general particle source (GPS) was set to generate an electron beam in the Z-direction with a radius of 2 mm, the energy of 6 MeV, and the standard deviation of energy of 500 keV. After the electron beam travelled through a 10 mm long cylindrical vacuum with a radius of 20

Table 1. Information about Materials

Material	Atomic fraction (%)						Chemical formula	Length (mm)	Density (g/cm^3)	w/wo Acryl box
	Hydrogen (H)	Carbon (C)	Nitrogen (N)	Oxygen (O)	Fluorine (F)	Chlorine (Cl)				
Lead	-	-	-	-	-	-	Pb	40	11.35	X
Iron	-	-	-	-	-	-	Fe	60	7.87	X
Tungsten	-	-	-	-	-	-	W	17	19.30	X
Titanium	-	-	-	-	-	-	Ti	80	4.54	X
Aluminium	-	-	-	-	-	-	Al	150	2.70	X
Bone (G4_BONE_COMPACT_ICRU - Geant4 material database)	-	-	-	-	-	-	-	220	1.85	O
Teflon	-	33.0	-	-	67.0	-	C_2F_4	150	2.20	X
Rubber (Neoprene)	5.7	54.3	-	-	-	40.0	C_4H_5Cl	170	1.23	X
Graphite	-	99.9	-	-	-	-	C	150	1.70	X
Paper	47.2	29.2	-	23.6	-	-	$C_6H_{10}O_5$	210	1.20	X
Ammonium acetate	58.0	17.2	8.0	16.8	-	-	$C_2H_7NO_2$	200	1.17	O
Polyethylene	66.4	33.6	-	-	-	-	C_2H_4	150	0.93	X
Acetamide	55.2	22.8	10.8	11.2	-	-	C_2H_5NO	150	1.16	O
Acryl [18] (polymethyl methacrylate)	8.5	59.3	-	32.2	-	-	$C_5H_8O_2$	5	1.18	-
HDPE (high-density polyethylene)	66.4	33.6	-	-	-	-	C_2H_4	-	0.96	-
Aluminium alloy (Al6061) [19]	-	-	-	-	-	-	-	2	2.70	-
X-ray scintillator ($CdWO_4$)	-	-	-	-	-	-	-	-	7.90	-
Neutron scintillator (plastic scintillator)	51.8	48.2	-	-	-	-	C_2H_4	-	1.096	-

w/wo, with/without.

mm, it collided with the tungsten target with a radius of 20 mm and a thickness of 2 mm. Subsequently, bremsstrahlung X-rays were produced. A lead collimator in the shape of a cylinder with a radius of 350 mm and a length of 300 mm was placed at the tip of the target for shielding. There was a 10 mm thick slit in the collimator that allowed the X-rays to have a vertical fan beam shape.

As aforementioned, the neutrons generated from the neutron generator have a slightly anisotropic angular distribution. In the simulation, neutrons with an energy of 14.1 MeV were generated isotropically from a point source on the target of the neutron generator using GPS, as the anisotropic angular distribution of neutrons emitted from the neutron generator is considered to have a negligible effect [17]. The HDPE collimator of a cuboid structure with a size of 1,800 mm × 2,170 mm × 2,400 mm (width × depth × height) has a cuboid space of 1,100 mm × 200 mm × 200 mm in which the neutron generator is located, and a slit with a thickness of 40 mm.

An air-cargo container with a size of 1,500 mm × 1,500 mm × 1,450 mm was located on the moving system and was approximately 1.1 m from the ground. A phantom for material discrimination was placed inside a container made of aluminium alloy (Al6061), with an outer wall thickness of 2 mm. We prepared phantoms of various materials in solid, liquid, and powdered form, and the powdered material was contained in a 5 mm thick acrylic (polymethyl methacrylate) box. The phantoms were 200 mm × 250 mm (width × height) in size. The materials belonging to metals, organic, and inorganic materials were selected. In addition, the materials were chosen to be evenly distributed in *R*-value, from low to high. The material information of the phantoms used to acquire the radiation images in the simulations is shown in Table 1 [18, 19]. The bone, ammonium acetate, and acetamide were in powder form, while the rest were in solid form.

A sensitive detector with a total size of 2,560 mm × 2,560 mm (width × depth) and 256 horizontally and vertically arranged scintillators with a size of 10 mm × 10 mm × 10 mm (width × depth × height) to detect radiation was placed behind the container. The detector material was composed of $CdWO_4$ for X-rays and plastic (EJ-276G; Eljen Technology) for neutrons [20].

As shown in Fig. 3, the radiation source, air-cargo, phantom, and detector were located in the Z-direction, and each distance from the radiation source was the same as that in the experimental condition. Thus, the world volume was filled with air.

2) Physics model

The physics models that should be considered in the process of radiation image acquisition using X-rays and neutrons

https://doi.org/10.14407/jrpr.2023.00080

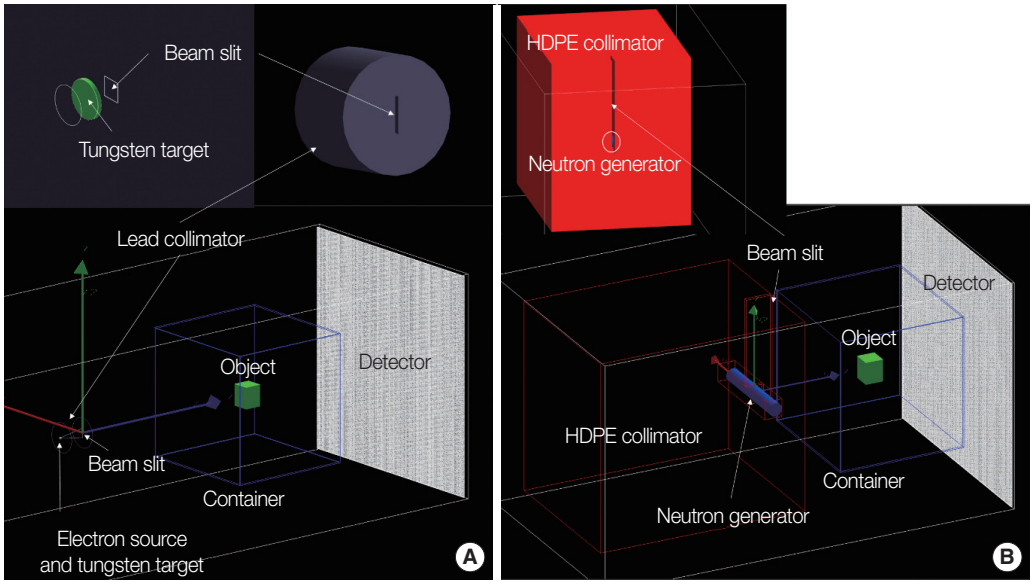

Fig. 3. Geometry setup for the (A) X-ray and (B) neutron system. HDPE, high-density polyethylene.

primarily involve the interactions of electrons with targets, photons with materials, and neutrons with materials.

First, the accelerated electrons from the linac collide with a target and bremsstrahlung X-rays are emitted. In this process, photons are emitted with energy as that of the energy loss of electrons owing to bremsstrahlung in the Coulomb field of the nucleus.

Second, the X-rays emitted by the X-ray generator interact with the collimator, air-cargo, phantom, and other equipment. X-rays, which are photons, are absorbed or scattered by interaction with matter, and the photoelectric effect, Rayleigh scattering (coherent scattering), Compton scattering (incoherent scattering), and pair production can occur. Considering the energy of photons emitted by electrons with a peak energy of 6 MeV, these photons interact with the bound electrons in the nucleus. Thus, the photons have a low probability of pair production and a high probability of photoelectric effect and Compton scattering.

Finally, because neutrons are electrically neutral, they interact with the nuclei of matter, and it depends on the energy of neutrons and the cross-section of the nuclide. Neutrons are scattered by the nuclei of matter and pass through the matter or slow down until they reach thermal energy (≤ 0.025 eV). In inelastic scattering, some of the neutron energy excites the nuclei, which then return to a stable state by emitting one or more gamma rays. When neutrons are sufficiently decelerated, they are captured by the nucleus, while protons, alpha particles, or gamma rays are emitted. Neutrons are highly sensitive to matter composed of light atoms, such as hydrogen, carbon, and oxygen, and have a high probability of interaction. The HDPE collimator, composed of hydrogen and carbon, produces many gamma rays during the process of scattering or capturing very fast neutrons with an energy of 14.1 MeV.

The physics model therefore includes the EmStandard_option4 and QGSP_BIC, which cover the reactions of charged particles, hadrons, and photons. Cutmore et al. [21] reported material discrimination results obtained using neutrons and cobalt-60 gamma rays. To confirm that the physic model was properly set, we reconstructed the results of the material discrimination for [21], and confirmed that the physics model was applied for radiation image acquisition.

3) Radiation image

In consideration of the resolution of the radiation image and the simulation running time, a total 10^7 particles were generated with the electron and neutron GPS, respectively. The initial number of particles was an unimportant parameter because material discrimination was performed using the relative contrast in gray-scale images. Radiation interacts with an air-cargo, phantom, etc., and only the transmitted radiation enters the detector with material information. When an event occurs in which radiation enters the detector from the world volume, the radiation is counted for each pixel, and an image of the phantom is obtained. The radiation images were also acquired in an environment without a phantom

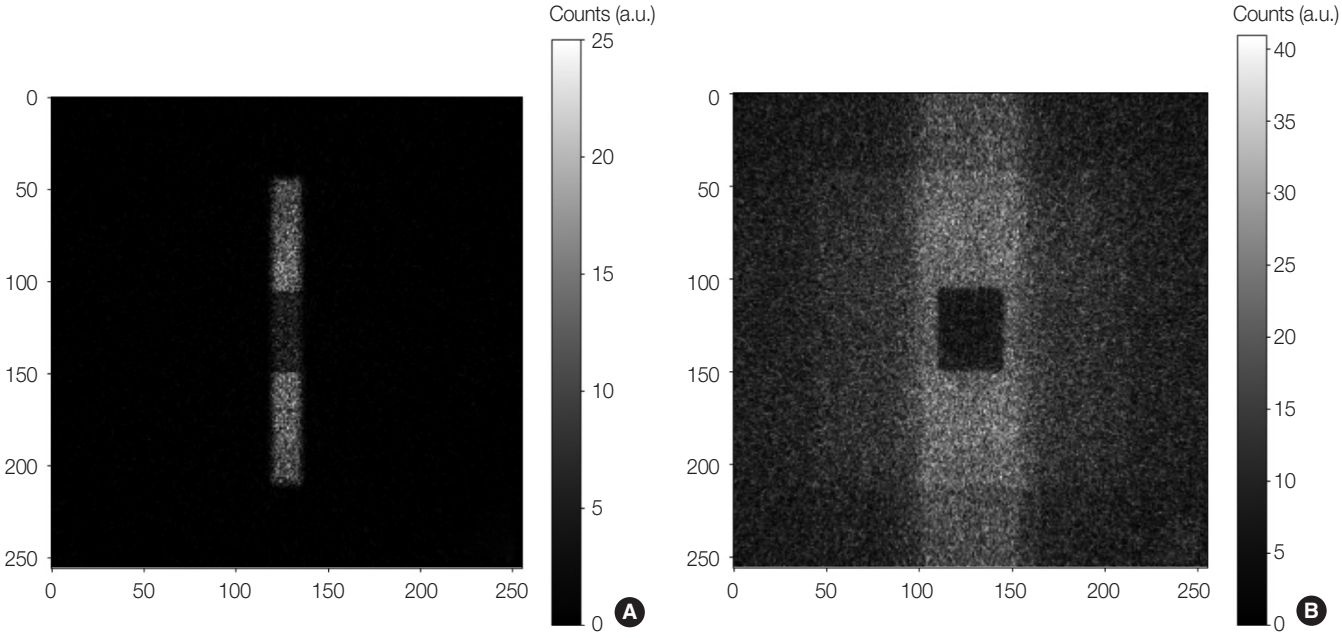

Fig. 4. (A) X-ray and (B) neutron image for the polyethylene phantom.

in order to calculate the ratio of signals with and without the phantom.

Fig. 4 shows images of X-ray and neutrons for a polyethylene phantom obtained by the simulation. In the image, the center black square object is the phantom inside the air-cargo container. The X-rays were completely shielded by the collimator, and only an image passing through the slit space was obtained. However, the neutrons were scattered by the collimator, as well as the slit was relatively wider than that of the X-rays, thus, an image of the entire phantom was obtained.

In the experiment, because the image was acquired while the phantom was moved by the moving system, a clear overall image was obtained. In this study, the movement of the phantom in the simulations was not considered because the intensity (number) of the incident radiation with material information on the detector was used for material discrimination. Only the image information in the center of the two columns was used for material discrimination, as in the experiment. We plan to conduct a simulation that considers the movement of the phantom in future research.

Results and Discussion

A parameter R, defined as the ratio of the attenuation coefficients of gamma rays and neutrons to a material, provides a criterion for distinguishing different classes of materials. The attenuation coefficients of mono-energetic neutrons and

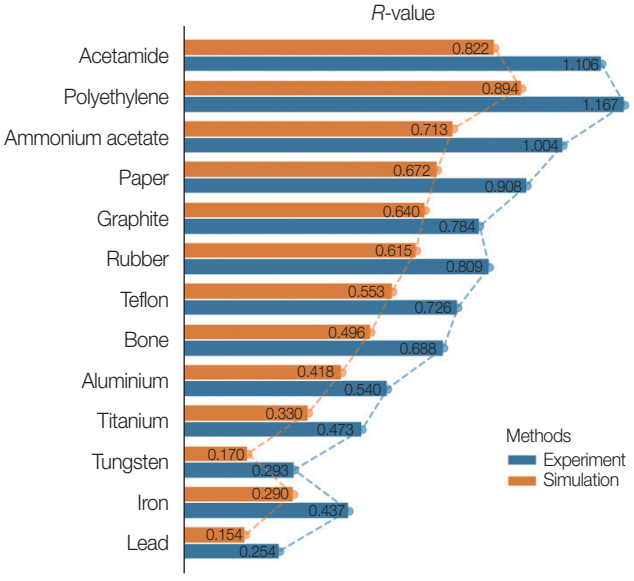

Fig. 5. Comparison of R-value for 13 phantoms. Blue color represents the result obtained by experiments and orange one represents the result obtained by simulations.

gamma rays are expressed as follows:

$$I_n = I_{n,0}e^{-(\mu_n/\rho)x},\ I_g = I_{g,0}e^{-(\mu_g/\rho)x} \quad (1)$$

where I_g and I_n are the measured radiation intensities through the matter, $I_{g,0}$ and $I_{n,0}$ are the measured radiation intensities without matter, and ρ and x are the density and thickness of the matter. Therefore, the parameter R is expressed as follow [21].

https://doi.org/10.14407/jrpr.2023.00080

$$R=\frac{\mu_n}{\mu_g}=\frac{ln\left(I_n/I_{n,0}\right)}{ln\left(I_g/I_{g,0}\right)} \quad (2)$$

Based on the radiation images obtained by experiments and simulations, the *R*-values for the 13 phantoms are shown in Fig. 5. In the graph of Fig. 5, the blue and orange colors show the *R*-values calculated from the radiation images obtained by experiments and simulations, respectively. For the 13 materials shown in Table 1, the *R*-values obtained in the experiments were greater than those obtained in the simulations. However, the trend of the *R*-value change for the 13 materials was similar. The difference of results is suspected to be due to the scattering of neutrons by the surrounding facilities and the neutron signal processing. The simulation is composed of only the neutron generator, the collimator, the phantom, the air-cargo container, and detectors, unlike the experiment. However, in the experiments, there are many facilities or equipment, and it is considered that this causes a lot of neutron scattering. In particular, the collimator for neutron generator is only made of HDPE, which is not capable of effectively shielding neutrons and acts as a large gamma ray source. As can be seen in Fig. 4, neutrons were detected throughout the image of the neutron, unlike the X-ray image. The other reason is the neutron signal processing. In the simulation, the intensity of the neutron signal is sum of the number of neutrons entering the detector. However, in the experiments, the neutron signal is obtained by detecting and superimposing the intensity of visible light caused by the reaction of neutrons and scintillators with the SiPM. Neutron detectors also detect gamma rays, and use a PSD technique to distinguish the two types of radiation. When the neutron detector detects a significant amount of gamma rays, it is difficult to distinguish the two types of radiation by threshold in the PSD scatter plot, so the neutron signal cannot be clearly separated. By improving the resolution of neutron images and obtaining *R*-values that match the experiment through more sophisticated simulations, the radiation images acquired by simulation can be used as training data for AI.

Conclusion

The KAERI has developed air-cargo security inspection equipment using X-rays and neutrons. The equipment acquires X-ray and neutron images of various objects, and also obtains information on materials constituting objects by differences in the characteristics of these radiations interacting with materials. We reconstructed the screening inspection equipment and calculated *R*-values from the radiation images for 13 materials using Geant4, a simulation toolkit based on the Monte Carlo method. We compared it with the *R*-value obtained in the experiment, and the results for material discrimination showed a similar tendency. Therefore, we confirmed the feasibility of using the radiation images acquired by simulation. The difference in the results can be suspected to be due to the following two causes. The first reason is that there are various facilities or equipment in the experimental environment that scatter neutrons, unlike in the simulation. The other is the difference in neutron signal processing. In the simulation, the neutron signal is the sum of the number of neutrons entering the detector. However, in the experiment, the neutron signal is obtained by superimposing the intensities of the neutron signals. Neutron detectors also detect gamma rays, and the neutron signal cannot be discriminated precisely in the process of separating the two types of radiation.

In the future, we plan to redesign the neutron collimator to reduce the significant amount of neutron scattering and gamma ray emission. We also plan to acquire radiation images by building a more realistic experimental environment in the simulation. By further research to improve the resolution of neutron image and overcome the difference between the experimental and simulation results, we can support the use of radiation images acquired by simulation, which can be used in a variety of fields. For example, neutron images can be used as training data of AI for material discrimination. However, the acquisition of a single neutron image using our security inspection equipment takes at least a few minutes, which means that considerable time and effort is required to train AI on the neutron image data. AI research using radiation image is being actively conducted in many fields, such as medicine, industry, and security. By using simulation-based radiation images, it is expected that it will be possible to easily obtain the training data of AI and achieve efficient research and development in the related fields.

Conflict of Interest

No potential conflict of interest relevant to this article was reported.

Acknowledgements

This study was supported by the Korea Atomic Energy Re-

search Institute (KAERI) Institutional R&D Program (Project No. 524450-23 and 523430-23) and this study was presented at the International Conference on Nuclear Analytical Techniques in 2022 (NAT2022), which was held in Daejeon, Korea, from December 7 to 9, 2022.

Ethical Statement

This article does not contain any studies with human participants or animals performed by any of the authors.

Author Contribution

Conceptualization: Lee J, Park J, Park JY, Chae M, Mun J. Data curation: Lee J, Park JY, Chae M, Mun J. Formal analysis: Lee J, Park J, Park JY. Supervision: Lee J, Park J, Park JY. Funding acquisition: Jung JH. Project administration: Lee J, Park JY, Chae M, Mun J. Investigation: Lee J. Resources: Lee J. Software: Lee J, Park J. Validation: Lee J, Park J. Writing - original draft: Lee J. Writing - review & editing: all authors. Approval of final manuscript: all authors.

References

1. Ford J, Faghri A, Yuan D, Gayen S. An economic study of the US post-9/11 aviation security. Open J Bus Manag. 2020;8(5):1923–1945.
2. Abidi BR, Zheng Y, Gribok AV, Abidi MA. Improving weapon detection in single energy X-ray images through pseudocoloring. IEEE Trans Syst Man Cybern C Appl Rev. 2006;36(6):784–796.
3. Martz HE, Glenn SM. Dual-energy X-ray radiography and computed tomography. 4th ed. Lawrence Livermore National Laboratory; 2019 [cited 2023 Nov 23]. Available from: https://www.osti.gov/servlets/purl/1608919
4. Sardet A, Perot B, Carasco C, Sannie G, Moretto S, Nebbia G, et al. Performances of C-BORD's tagged neutron inspection system for explosives and illicit drugs detection in cargo containers. IEEE Trans Nucl Sci. 2021;68(3):346–353.
5. Akcay S, Kundegorski ME, Willcocks CG, Breckon TP. Using deep convolutional neural network architectures for object classification and detection within X-ray baggage security imagery. IEEE Trans Inf Forensics Secur. 2018;13(9):2203–2215.
6. Naresh K, Khan KA, Umer R, Cantwell WJ. The use of X-ray computed tomography for design and process modeling of aerospace composites: a review. Mater Des. 2020;190:108553.
7. van Kaick G, Delorme S. Computed tomography in various fields outside medicine. Eur Radiol. 2005;15 Suppl 4:D74–D81.
8. Kolkoori S, Wrobel N, Deresch A, Redmer B, Ewert U. Dual high energy X-ray digital radiography for material discrimination in cargo containers. Proceedings of the 11th European Conference on Non-Destructive Testing (ECNDT 2014); 2014 Oct 6–10; Prague, Czech Republic.
9. Lee D, Lee J, Min J, Lee B, Lee B, Oh K, et al. Efficient material decomposition method for dual-energy X-ray cargo inspection system. Nucl Instrum Methods Phys Res A. 2018;884:105–112.
10. Gustschin A, Neuwirth T, Backs A, Viermetz M, Gustschin N, Schulz M, et al. Comparison of thermal neutron and hard X-ray dark-field tomography. J Imaging. 2020;7(1):1.
11. Eberhardt JE, Rainey S, Stevens RJ, Sowerby BD, Tickner JR. Fast neutron radiography scanner for the detection of contraband in air cargo containers. Appl Radiat Isot. 2005;63(2):179–188.
12. Gozani T. The role of neutron based inspection techniques in the post 9/11/01 era. Nucl Instrum Methods Phys Res B. 2004;213:460–463.
13. Liu Y, Sowerby BD, Tickner JR. Comparison of neutron and high-energy X-ray dual-beam radiography for air cargo inspection. Appl Radiat Isot. 2008;66(4):463–473.
14. Mun J, Chae M, Lee J, Yeon YH, Park JY, Lee NH. Design and fabrication of side-coupled RF cavity for S-band 6/3 MeV dual-energy electron linac. J Korean Phys Soc. 2022;80(7):558–569.
15. Park YJ, Mun J, Lee JH, Yeon YH, Chae M, Lee M, et al. Development of a dual-modality gamma ray/fast neutron imaging system for air cargo inspection. Appl Sci. 2022;12(19):9775.
16. Agostinelli S, Allison J, Amako K, Apostolakis J, Araujo H, Arce P, et al. Geant4: a simulation toolkit. Nucl Instrum Methods Phys Res A. 2003;506(3):250–303.
17. Czakoj T, Kostal M, Zmeskal M, Novak E, Mravec F, Cvachovec F, et al. The characterization of D-T neutron generators in precise neutron experiments. Nucl Instrum Methods Phys Res A. 2022;1034:166837.
18. Liou H, Liou W, Lin H, Hwu Y, Chen W. Characterization of gold/PMMA hybrid nanomaterials synthesized by hard X-ray synchrotron radiation. Particuology. 2010;8(3):234–239.
19. Ekambaram S, Murugan N. Synthesis and characterization of Aluminium alloy AA6061-Alumina metal matrix composite. Int J Curr Eng Technol. 2015;5(5):3211–3216.
20. Grodzicka-Kobylka M, Szczesniak T, Moszynski M, Brylew K, Swiderski L, Valiente-Dobon JJ, et al. Fast neutron and gamma ray pulse shape discrimination in EJ-276 and EJ-276G plastic scintillators. J Instrum. 2020;15:P03030.
21. Cutmore NG, Liu Y, Sowerby BD, Tickner JR, Peng H, Xie Y. SM/EN-01: Recent developments in fast neutron radiography for the interrogation of air cargo containers. Proceedings of International Topical Meeting on Nuclear Research Applications and Utilization of Accelerators; 2009 May 4–8; Vienna, Austria. p. 136.

 https://doi.org/10.14407/jrpr.2023.00080